

## Subpicosecond hot-hole relaxation in germanium studied by time-resolved inter-valence-band Raman scattering

Koichiro Tanaka,\* Hideyuki Ohtake,† Hiroyuki Nansei, and Tohru Suemoto  
*Institute for Solid State Physics, University of Tokyo, Tokyo 106, Japan*

(Received 2 June 1995)

Buildup of the Raman signal due to inter-valence-band scattering of holes was observed in the subpicosecond time scale in germanium. The buildup is attributed to the increase of holes at  $k \simeq 7.9 \times 10^6 \text{ cm}^{-1}$ , reflecting the cooling process. By analysis, taking the optical-phonon scattering into account, the deformation potential is obtained as  $D_0 = 1.0 \times 10^9 \text{ eV/cm}$ .

Interband and intraband relaxation are essentially important for the nonequilibrium dynamics of hot carriers in semiconductors in the ultrafast time region. Several techniques were applied to clarify the dynamics, such as transient absorption measurements<sup>1</sup> and luminescence spectroscopy by sum-frequency generation.<sup>2-4</sup> However, most of the techniques have the disadvantage that the obtained data reflect not only hot electrons but also hot holes and therefore we cannot obtain the relaxation process of each carrier separately. A Raman scattering technique seems a good method to overcome this, because it gives information of the elementary excitation in a frequency domain and separates them by selection rules.<sup>5</sup> From this point of view, a time-resolved Raman scattering technique based on the pump-probe method has been used to clarify the carrier cooling process. For example, in several III-V semiconductors such as GaAs, time evolution of the hot phonon population after making photoexcited carriers was observed by monitoring the anti-Stokes Raman intensity due to LO phonons.<sup>6-8</sup> However, by this method, the information on the carrier cooling process is obtained indirectly through the carrier-phonon kinetics.

Recently we made time-resolved *electronic* Raman scattering measurements in Ge with 110 fs time resolution, which have the merit of giving us direct information on the carrier relaxation process.<sup>9</sup> We utilized an electronic Raman component which has an asymmetric spectrum centered at the laser frequency in order to monitor the dynamics of photoexcited electrons. The origin is attributed to the intervalley density fluctuation (IVF) of photoexcited electrons. We found that the initial symmetric spectrum of the IVF becomes asymmetric within 4 ps, which means that the temperature of the electrons is cooled down within 4 ps. The intensity of the Raman signal was found to increase with a time constant of 1.2 ps. From the result, we concluded that photoexcited electrons initially created in the  $\Gamma$  valley are scattered into  $L$  valleys with a time constant of 1.2 ps. In the experiment we cannot obtain any information on the relaxation process of photoexcited holes.

In this paper, we present the first (to our knowledge) time-resolved inter-valence-band Raman scattering (TR IVRS) measurements in germanium and discuss the thermalization and cooling process of hot holes.

An undoped germanium sample with a (100) face

was investigated at 300 K. The measurement system of the time-resolved Raman scattering has been reported elsewhere.<sup>9</sup> 110 fs pulses from a Ti:sapphire laser were split into two beams, which have polarization perpendicular to each other. The beams are focused with a diameter of 30  $\mu\text{m}$  on the sample surface. The one beam is used to excite hot carriers in Ge and the other is to measure Raman spectra. The power density of both beams is 3.6  $\text{kW/cm}^2$ , which corresponds to the carrier density of  $p_0 = 3 \times 10^{18} \text{ cm}^{-3}$  per pulse. From the absorption coefficient, carriers are generated within 150 nm in depth.

Figures 1(a) and 1(b) show typical Raman spectra under cw laser excitation with different excitation densities. In the low density case [Fig. 1(b)], one can see Raman scattering lines due to LO phonon around  $\pm 300 \text{ cm}^{-1}$  with two-LO-phonon lines around  $\pm 600 \text{ cm}^{-1}$ . In Fig. 1(a), in addition to them, there are broad scattering components which depend on the laser power nonlinearly. Their origins are already assigned: the scattering around  $0 \text{ cm}^{-1}$  is attributed to the IVF of  $L$ -valley electrons mentioned above<sup>9-11</sup> and the scattering around  $1500 \text{ cm}^{-1}$  is due to photoexcited holes; the scattering mechanism is assigned as a resonant inter-valence-band Raman scattering (resonant IVRS) of holes: holes are scattered from the heavy-hole band to the light-hole band where the

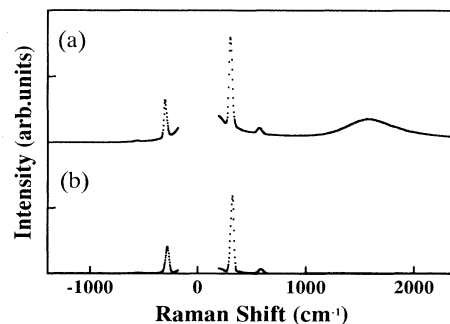


FIG. 1. Typical Raman spectrum of undoped Ge sample at 300 K under cw excitation of 1.58 eV light with a density of (a) 18.6  $\text{kW/cm}^2$  and (b) 0.14  $\text{kW/cm}^2$ . Polarization of the scattered light was taken as parallel to that of the incident laser (parallel to the  $\langle 110 \rangle$  crystal axis). Lack of the data around  $0 \text{ cm}^{-1}$  is due to the Raman notch filter. Spectral resolution is about  $24 \text{ cm}^{-1}$ .

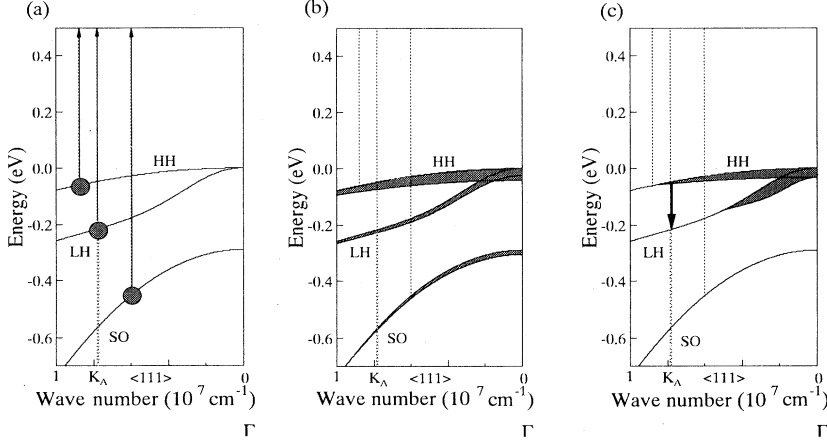


FIG. 2. Schematic illustration of the relaxation processes of hole gas. (a) Holes are photoexcited at special points in the dispersion curves. (b) Photoexcited holes are quickly spread over three hole bands and thermalized with temperature  $T_h(0)$ . (c) The temperature of hole gas is cooled down by emission of optical phonons. The arrow shows the scattering of holes from HH to LH by the resonant IVRS.

energy separation between the light-hole band and the conduction band is the same as the photon energy of the incident laser light.<sup>12</sup> The situation is schematically shown in Fig. 2(c) by the arrow. We focused on the scattering around  $1500 \text{ cm}^{-1}$  and made subpicosecond time-resolved experiments.

Figure 3 shows typical time-resolved Raman spectra around  $1500 \text{ cm}^{-1}$  at several delay times after injection of photoexcited carriers. At 0 ps, one cannot see the resonant IVRS component so clearly but only a strong background component due to the IVF. As the delay time increases, the intensity of the IVRS component becomes large. The intensities of the IVRS component are plotted against delay times in Fig. 4. The Raman intensity reaches a maximum around 3 ps and then decreases slowly. In Ref. 12, we presented the scattering model and showed that the Raman intensity  $I_{\text{Raman}}$  should be proportional to the hole occupation number at the resonant position [wave number  $K_A$  shown in Fig. 2(a)]. The most important contribution comes from the holes, whose wave vector is parallel to the  $\langle 111 \rangle$  direction. Therefore the Raman intensity can be written by Eq. (1) under

Fermi-Dirac statistics.

$$I_{\text{Raman}} \propto f_h(E_h(K_A)) = \frac{1}{e^{\frac{E_h - \mu_h(t)}{k_B T_h(t)}} + 1}, \quad (1)$$

where  $E_h(K_A)$  is the energy of the heavy hole at the resonant position;  $T_h(t)$  and  $\mu_h(t)$  represent the time-dependent temperature of photoexcited hole gas and Fermi energy; the latter depends on temperature and density of holes. From Eq. (1), we can say that the Raman intensity increases when  $\mu_h$  decreases under  $T(t) = \text{const}$ . Decrease of  $\mu_h$  corresponds to the decrease of the density of hole gas. From this point, it is strongly suggested that the slow decay of the Raman signal after 5 ps reflects a decrease of the carrier density. Photoexcited carriers initially locate near the surface. They should escape from the excited region by diffusion. In fact, by using diffusion constant of holes at 300 K ( $46 \text{ cm}^2/\text{sec}$ ),<sup>13</sup> we can show that the hole density is nearly constant until 5 ps after injection of the laser light and holes are diffused over in the longitudinal direction after 5 ps. It is well known that one-dimensional diffusion makes the carrier density decrease as  $t^{-0.5}$ , which agrees with the decrease of experimental data after 5 ps shown in Fig. 4.

As for the initial rise of the Raman intensities, we propose a model that the cooling of holes makes the hole occupation number at the resonant position increase. In order to confirm this model, we made quantitative calcu-

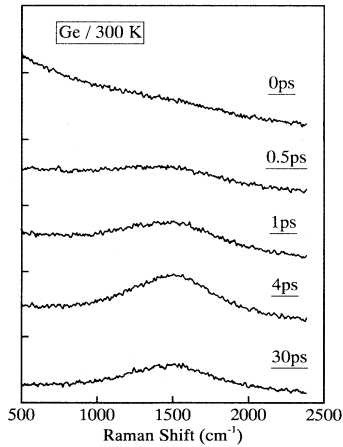


FIG. 3. Time-resolved Raman spectra of the  $1500 \text{ cm}^{-1}$  component. As the delay time is increased, the intensity of the  $1500 \text{ cm}^{-1}$  component increases and after 5 ps slightly decreases.

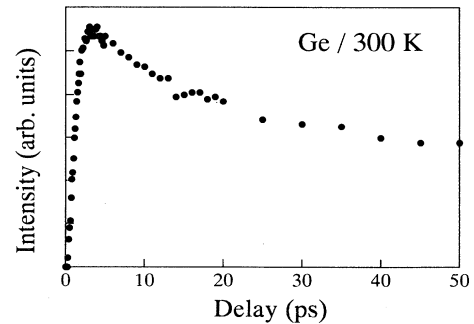


FIG. 4. Time evolution of the integrated intensity of the  $1500 \text{ cm}^{-1}$  component.

lations based on four assumptions.

(1) After creation of electron-hole pairs by the pump pulse [Fig. 2(a)], the hole system quickly thermalized via hole-hole ( $h-h$ ) and electron-hole ( $e-h$ ) scattering within the pulse width of the pump light to a Fermi-Dirac distribution with the initial hole temperature  $T_h(0)$  and Fermi energy  $\mu_h(0)$  [Fig. 2(b)].

(2) The hole system cools down through the emission process of optical phonons [Fig. 2(c)].

(3) Quasiequilibrium is always kept via fast  $h-h$  and  $e-h$  scattering processes.

(4) The hole density is constant, which means that the Fermi energy depends only on the temperature when the delay time is shorter than 5 ps.

The assumption of (1) and (3) are based on the well-known result that the  $e-e$ ,  $h-h$ , or  $h-e$  scattering is much shorter than 100 fs in the high density region ( $p_0 > 10^{17} \text{ cm}^{-3}$ ).<sup>4,14</sup>

In the following, we made a simple calculation, taking heavy-hole and light-hole bands into account after Woener *et al.*<sup>15</sup> The average energy of the hole system can be written as [Eq. (3) in Ref. 15]

$$\langle E(T_h(t)) \rangle = \frac{1}{p_0} \int_0^\infty ED(E)f_h(E)dE, \quad (2)$$

where  $f_h(E)$  is the Fermi-Dirac distribution function depending on  $T_h(t)$  and  $\mu_h(t)$ ,  $D(E)$  is the sum of the density of states of the heavy-hole and light-hole bands, and  $p_0$  is the hole density:

$$p_0 = \int_0^\infty D(E)f_h(E)dE. \quad (3)$$

We approximate the band structure by parabolic dispersion relations and we use a  $\vec{k}$ -independent optical deformation potential characterized by a coupling constant  $D_0$  to account for both intra- and inter-band phonon scattering. The average energy loss per hole with carrier temperature  $T_h$  is given by<sup>15</sup>

$$\begin{aligned} \left\langle \frac{dE}{dt}(T_h) \right\rangle_{\text{loss}} &= \frac{\hbar\omega_0}{p_0} \int_{\hbar\omega_0}^\infty D(E)f_h(E) \\ &\quad \times [1 - f_h(E - \hbar\omega_0)] W_{\text{emi}}(E) dE \\ &\quad - \frac{\hbar\omega_0}{p_0} \int_0^\infty D(E)f_h(E) \\ &\quad \times [1 - f_h(E + \hbar\omega_0)] W_{\text{abs}}(E) dE, \quad (4) \end{aligned}$$

where  $W_{\text{emi}}(E)$  and  $W_{\text{abs}}(E)$  are phonon emission and absorption rates of a hole, which are proportional to the deformation potential  $D_0$  and are defined in Ref. 15 [Eq. (5) and Eq. (6)].  $\omega_0$  is the optical phonon energy (37 meV). For the numerical calculation, we introduce the heat capacity  $c(T_h)$  of the hole gas, which is defined as

$$c(T_h) = \frac{d\langle E(T_h) \rangle}{dT_h}. \quad (5)$$

With the above definitions, the following differential equation for the temperature of holes is derived:

$$c(T_h) \frac{dT_h}{dt} = - \left\langle \frac{dE}{dt}(T_h) \right\rangle_{\text{loss}}. \quad (6)$$

The hole temperature  $T_h$  is obtained by a stepwise integration of Eq. (6). After each  $\delta t = 20$  fs, the Fermi level of holes  $\mu_h(t)$ , which depends on  $T_h(t)$ , the heat capacity, and the energy loss, are calculated by Eqs. (3)–(5). We hold the hole density  $p_0$  fixed under the calculations. By using these values, we calculate the hole temperature  $T_h(t + \delta t)$  at each step.

The initial temperature was determined as  $T_h(0) = 3000$  K from the weighted average of the kinetic energy of holes at the initially excited positions shown in Fig. 2(a). The Fermi energy of the hole gas at  $t = 0$  was also determined as  $\mu_h(0) = -0.78$  eV by using the initial hole density  $p_0 = 3 \times 10^{18} \text{ cm}^{-3}$  and  $T_h(0) = 3000$  K.

Typical results of the time evolution of  $T_h(t)$  are given in Fig. 5(a) for  $D_0 = 0.9 \times 10^9$  eV/cm,  $D_0 = 1.0 \times 10^9$  eV/cm, and  $D_0 = 1.1 \times 10^9$  eV/cm. One can see the faster cooling process of the hole gas for the larger deformation potential  $D_0$ . The Raman intensity can be calculated from Eq. (1) by using  $T_h(t)$  and  $\mu_h(t)$ . Results for three  $D_0$ 's are shown in Fig. 5(b) with data points (closed circles). The solid curve ( $D_0 = 1.0 \times 10^9$  eV/cm) can reproduce the data quite well as long as the delay is set beyond 700 fs. The value  $D_0 = 1.0 \times 10^9$  eV/cm is very close to the value reported in Ref. 16 ( $0.9 \times 10^9$  eV/cm) and in Ref. 17 ( $1.2 \times 10^9$  eV/cm), which are determined from measurements of the hole mobility as a function of lattice temperatures. Therefore these results support our interpretation that the fast increase of the IVRS signal reflects the cooling process of hole gas through scattering due to optical phonons.

For the delay  $t < 700$  fs, all calculations go to the same value at  $t = 0$ , which depends on the initial conditions and deviates from data points. If we use an unreal high initial temperature such as  $T_h(0) = 10\,000$  K, we

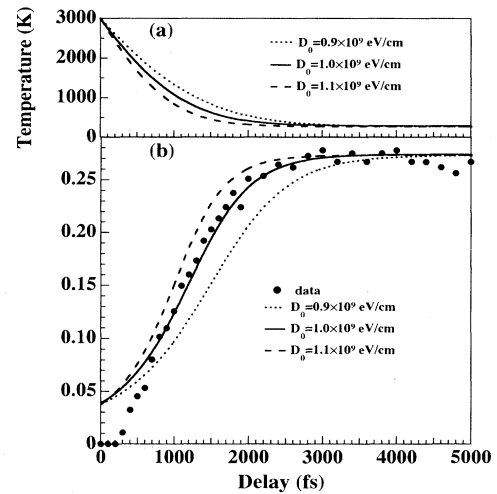


FIG. 5. (a) Calculated temperature cooling of hole gas in germanium for three deformation potentials. (b) Calculated time-evolution of the Raman intensity with data (closed circles). See text for the details of the calculation.

can obtain quite excellent fitting even for  $t < 700$  fs with  $D_0 = 1.0 \times 10^9$  eV/cm. The reason for the deviation is not clear at present but one possibility is that the assumption (1) mentioned above was incorrect for delay  $t < 700$  fs: the hole does not equilibrate well and the population should be localized at special positions in  $k$  space for  $t < 700$  fs and the equilibrating process gives rise to a rise of the Raman intensity from zero.

Recently Woener *et al.* reported a slightly smaller deformation potential,  $D_0 = 6.3 \times 10^8$  eV/cm.<sup>15</sup> They made infrared pump and probe experiments in  $p$ -type germanium with the hole concentration between  $10^{16}$  and  $10^{17}$ . In their case, holes are initially in the heavy-hole band and light-hole band. The infrared pump beam brings heavy holes to the light-hole band or light holes to the split-off hole band and makes the hole gas hot. In order to determine  $D_0$ , they made experiments at 30 K and utilize data between 5 ps and 40 ps when the temperature varies from 300 K to 30 K. This means that they mon-

itor the cooling process of holes near the  $\Gamma$  point where the scattering by optical phonons is more ineffective than the scattering by acoustic phonons. On the contrary, we can monitor higher temperature of hole gas where the optical-phonon-scattering process is dominant. Such a difference in the temperature region will give rise to a difference of  $D_0$  between Woener's and ours.

In conclusion, we observed buildup of the Raman signal due to interband scattering of holes in the subpicosecond time scale in germanium. The buildup is attributed to the increase of holes at the initial state, which reflects the cooling process. From the calculation based on several assumptions, we obtained the deformation potential as  $D_0 = 1.0 \times 10^9$  eV/cm.

This work was partially supported by the Grant-In-Aid for Scientific Research from the Japanese Ministry of Education, Science and Culture, and also by the Murata Science Foundation.

\* Present address: Hirao Active Glass Project, ERATO, JRDC, Keihanna-Plaza, Hikaridai, Kyoto 619-02, Japan.

† Permanent address: Science University of Tokyo, Tokyo 162, Japan.

<sup>1</sup> J.-Y. Bigot, M. T. Portella, R. W. Schoenlein, J. E. Cunningham, and C. V. Shank, *Phys. Rev. Lett.* **65**, 3429 (1990).

<sup>2</sup> J. Shah, B. Deveaud, T. C. Damen, W. T. Tsang, A. C. Gossard, and P. Lugli, *Phys. Rev. Lett.* **59**, 2222 (1987).

<sup>3</sup> J. Shah, in *Spectroscopy of Nonequilibrium Electrons and Phonons*, edited by C. V. Shank and B. P. Zakharchenya (North-Holland, Amsterdam, 1992), pp. 57–112.

<sup>4</sup> T. Elsaesser, J. Shah, L. Rota, and P. Lugli, *Phys. Rev. Lett.* **66**, 1757 (1991).

<sup>5</sup> For example, see *Light Scattering in Solids I*, edited by M. Cardona (Springer-Verlag, Berlin, 1983).

<sup>6</sup> J. A. Kash, J. C. Tsang, and J. M. Hvam, *Phys. Rev. Lett.* **54**, 2151 (1985).

<sup>7</sup> D. Kim and P. M. Yu, *Phys. Rev. B* **43**, 4158 (1991).

<sup>8</sup> D. Kim, J. M. Jacob, J. F. Zhou, J. J. Song, H. Hou, C. W. Tu, and H. Morkoç, *Phys. Rev. B* **45**, 13973 (1992).

<sup>9</sup> K. Tanaka, H. Ohtake, and T. Suemoto, *Phys. Rev. Lett.* **71**, 1935 (1993).

<sup>10</sup> G. Contreras, A. K. Sood, and M. Cardona, *Phys. Rev. B* **32**, 930 (1985).

<sup>11</sup> N. Mestres and M. Cardona, *Phys. Rev. Lett.* **55**, 1132 (1985).

<sup>12</sup> K. Tanaka, H. Ohtake, and T. Suemoto, *Phys. Rev. B* **50**, 10694 (1994).

<sup>13</sup> F. J. Morin, *Phys. Rev.* **93**, 62 (1954).

<sup>14</sup> L. Rota, P. Lugli, T. Elsaesser, and J. Shah, *Phys. Rev. B* **47**, 4226 (1993).

<sup>15</sup> M. Woerner, T. Elsaesser, and W. Kaiser, *Phys. Rev. B* **45**, 8378 (1992).

<sup>16</sup> M. Castato and L. Reggiani, *Phys. Status Solidi B* **53**, 471 (1973).

<sup>17</sup> D. M. Brown and R. Bray, *Phys. Rev.* **127**, 1593 (1962).